Environmental Science & Technology

pubs.acs.org/est

Article

Chemical Production of Oxygenated Volatile Organic Compounds Strongly Enhances Boundary-Layer Oxidation Chemistry and Ozone Production

Hang Qu, Yuhang Wang,* Ruixiong Zhang, Xiaoxi Liu, Lewis Gregory Huey, Steven Sjostedt, Limin Zeng, Keding Lu, Yusheng Wu, Min Shao, Min Hu, Zhaofeng Tan, Hendrik Fuchs, Sebastian Broch, Andreas Wahner, Tong Zhu, and Yuanhang Zhang

Cite This: *Environ. Sci. Technol.* 2021, 55, 13718−13727

Read Online

ACCESS | Metrics & More | Article Recommendations | Supporting Information

ABSTRACT: Photolysis of oxygenated volatile organic compounds (OVOCs) produces a primary source of free radicals, including OH and inorganic and organic peroxy radicals (HO_2 and RO_2), consequently increasing photochemical ozone production. The amplification of radical cycling through OVOC photolysis provides an important positive feedback mechanism to accelerate ozone production. The large production of OVOCs near the surface helps promote photochemistry in the whole boundary layer. This amplifier effect is most significant in regions with high nitrogen oxides (NO_x) and VOC concentrations such as Wangdu, China. Using a 1-D model with comprehensive observations at Wangdu and the Master Chemical Mechanism (MCM), we find that OVOC photolysis is the largest free-radical source in the boundary layer (46%). The condensed chemistry mechanism we used severely underestimates the OVOC amplifier effect in the boundary layer, resulting in a lower ozone production rate sensitivity to NO_x emissions. Due to this underestimation, the model-simulated threshold NO_x emission value, below which ozone production decreases with NO_x emission decrease, is biased low by 24%. The underestimated OVOC amplifier effect in a condensed mechanism implies a low bias in the current 3-D model-estimated efficacy of NO_x emission reduction on controlling ozone in polluted urban and suburban regions of China.

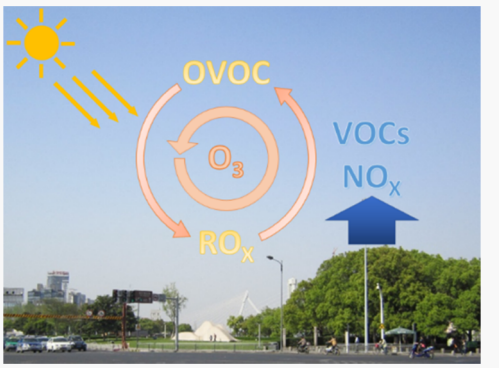

KEYWORDS: *ozone, photochemistry, oxygenated volatile organic compounds, organic peroxy radicals, chemical mechanism*

1. INTRODUCTION

Oxygenated volatile organic compounds (OVOCs) are omnipresent in the atmosphere and strongly affect atmospheric oxidation.[1−4] Photolysis of OVOCs is a primary source of the HO_x (OH + HO_2) and organic peroxy (RO_2) radicals, promoting the production of ozone and peroxyacetyl nitrate (PAN, $CH_3C(O)OONO_2$).[5−7] Ozone has adverse effects on human and vegetation health and is a greenhouse gas;[8,9] PAN formation and transport significantly enhance the impact of anthropogenic emissions in remote regions.[10,11] OVOCs also contribute to the formation of secondary organic aerosols (SOAs), which affect human health and regional climate.[12−14]

The oxidation of nonmethane hydrocarbons (NMHCs) is a major source of OVOCs.[15] The major sinks of OVOCs are photolysis and reactions with OH radicals. The observations of OVOCs provide important constraints on our understanding of VOC emissions and photochemistry. For example, the observed HCHO levels in wintertime over the northeastern United States indicate that the primary HCHO emission in the GEOS-Chem model was underestimated by over 75%.[16] In China, the OMI-observed glyoxal columns indicate that the aromatic emissions were underestimated and must be increased by a factor of 5−6.[17] In central Europe, the nonmethane VOC (NMVOC) and OVOC emissions must be increased by 2 and 3.8 times separately to match the measured NMVOC and OVOC fluxes in an urban area.[18] Other model studies also found underestimations of OVOC concentrations.[19−21]

There are other possible reasons that may explain the discrepancies between observed and simulated OVOCs. In addition to the uncertainties of chemical kinetics, the chemical mechanisms used in models have various degrees of complexity.[22−27] Compared to an explicit mechanism with several thousands of reactions, condensed mechanisms used in 3-D regional and global models usually have a selected subset of

Received: July 6, 2021
Revised: September 2, 2021
Accepted: September 29, 2021
Published: October 8, 2021

hundreds of reactions for the simulations of ozone and secondary aerosol formations.[16,17,21] The large reduction of the number of reactions greatly enhances the computational efficiency of model simulations but it can also adversely affect the simulations of OVOCs and the sources of radicals from OVOC photolysis.

When analyzing surface measurements of VOCs and OVOCs, box models are often used. However, vertical transport, which strongly enhances surface PAN concentrations and alters boundary-layer pollution distributions, is an important factor that cannot be properly represented in box model simulations.[7,28] In this study, we make use of the comprehensive observations from the 2014 field campaign at Wangdu, China, to constrain box and 1-D models with explicit and condensed chemistry mechanisms and investigate the effects of the model chemical mechanism and boundary-layer mixing on the simulations of OVOCs and their chemistry in light of the observations. We find that OVOCs in the boundary layer play a critical role in amplifying near-surface photochemical oxidation and ozone production.

2. METHODS

2.1. Observations. The Campaigns of Air Pollution Research in Megacity Beijing and North China Plain (CAREBEIJING-NCP) took place at a rural site near a small town, Wangdu (38.665°N, 115.204°E), in Hebei Province from June 7 to July 8, 2014 (Figure S1). The town of Wangdu has a population of 260 000, and there is no major industry. The closest large city of Baoding is located 35 km northeast of the measuring site. Major cities including Beijing, Tianjin, and Shijiazhuang are located 90−180 km away from the site. Multiple instruments were deployed in the campaign. Ozone was measured by ultraviolet (UV) absorption (Thermo Electron 49i). CO, CH_4, and H_2O were measured by a cavity ring-down (CRDS) instrument (Picarro G2401). NO and NO_2 were measured by the chemiluminescence method (Thermo Electron 42i) using a homebuilt photolytic converter to avoid interferences from other oxidized nitrogen compounds.[32] HONO was measured by long-path absorption photometry (LOPAP) using a homebuilt instrument from Peking University (PKU).[29] Fifty-nine VOCs were measured by a gas chromatograph (GC) attached with a flame ionization detector (FID) and a mass spectrometer (MS) from PKU.[30] Formaldehyde (HCHO) was measured by the Hantzsch fluorescence method (Aerolaser GmbH AL4021). PAN, Cl_2, and $ClNO_2$ were measured by a chemical ionization mass spectrometry (CIMS) instrument from the Georgia Institute of Technology.[31] OH, HO_2, and RO_2 were measured by a laser-induced fluorescence (LIF) technique from PKU.[32] The photolysis frequencies were calculated with the measured spectral actinic photon flux density using a spectroradiometer.[33] The aerosol surface area was calculated by the size distribution of the aerosols measured by a twin differential mobility particle sizer (TDMPS) and an aerodynamic particle sizer (APS).[34] Meteorology fields including temperature, pressure, relative humidity, wind speed, and wind direction were measured at 10 and 20 m in a 20 m tower. The time resolution and the uncertainties of the measurements used for this study are summarized in Table S1.

2.2. Model. In previous model studies, lumped chemistry mechanisms have been found to produce a similar result (within 10%) for ozone and other critical species.[35−37] We choose the GCM mechanism to represent the lumped mechanisms. The condensed GCM mechanism was taken from the GEOS-Chem model (v9-02), with an extended set of reactions involving aromatics, ethylene, and acetylene; it includes 110 active species and 400 reactions,[38] and the explicit chemical mechanism is a subset of the Master Chemical Mechanism (MCM 3.3.1) containing all measured species with 3500 species and 10 700 reactions.[22−27] We also modified both mechanisms to include eight Cl species and related inorganic and organic reactions, which have been described in detail before.[31] Observed photolysis rates of eight photolytic decomposition reactions of O_3, NO_2, NO_3 (two separate pathways), HONO, H_2O_2, and HCHO (two separate pathways) are used in modeling. For all of the other photolytic reactions, linear scaling factors are derived to compute these rates based on O_3 and NO_2 photolysis rates using FAST-J calculations.[39] We then apply the scaling factors to the observed O_3 and NO_2 photolysis rates to compute all other photolysis reaction rates. The observations of O_3, CO, CH_4, H_2O, NO, NO_2, HONO, VOCs, Cl_2, $ClNO_2$, temperature, pressure, and aerosol surface area (see Table S1 for additional information) are constrained in the box models and the surface layer of the 1-D models. Missing observation data are replaced by the average value at the same time of the day to allow for continuous simulation. The chemistry time step of the model is 1 min, and the observations with frequencies lower than once per minute are interpolated linearly. We selected and lumped 59 measured VOCs in the GCM model to preserve the OH reactivities in the two mechanisms (Text S1 and Table S2). The chemical solver uses the sparse matrix, vectorized gear (SMVGEAR) code.[40] The box model does not include deposition and dilution processes.

The 1-D model extends the box model into 30 vertical layers from the surface to the top of the troposphere, and the top height of each layer is listed in Table S3. The meteorology data including pressure, temperature, water vapor concentration, boundary-layer height, and vertical eddy diffusion coefficient are obtained from the Weather Research and Forecasting model (WRF) assimilations constrained by the National Centers for Environmental Prediction Climate Forecast System Version 2 (NCEP CFSv2) products.[41] The WRF domain is shown in Figure S2, and the boundary-layer height is shown in Figure S3. The 1-D model includes vertical mixing and dry deposition[6,42] based on WRF simulation results. The simulated vertical diffusion coefficients near the surface agree well with the data derived from surface flux measurements (Figure S4). The time step for vertical mixing is 1 min, the same as chemistry.

The data for dry deposition velocities and top chemical boundary conditions in the 1-D simulations are obtained from the 3-D REAM model result. The 3-D REAM model has a horizontal resolution of 36 km, and the vertical resolution of the 3-D REAM is the same as the 1-D model. The chemistry mechanism of the 3-D REAM is the same as the condensed mechanism. The 2012 Multi-resolution Emission Inventory for China (MEIC) emissions are adopted in the 3-D REAM for anthropogenic emissions of NO_x, VOCs, and CO.[43] The isoprene emissions in the 3-D REAM are calculated using the Model of Emissions of Gases and Aerosols from Nature (MEGAN v2.1).[44] We run the 3-D REAM model for the measurement period. A detailed description of the 3-D REAM model can be found in previous studies.[45−47] We use the average hourly profiles of the measurements to constrain box and 1-D models and spin up the model simulations for 10 days.

https://doi.org/10.1021/acs.est.1c04489
Environ. Sci. Technol. 2021, 55, 13718−13727

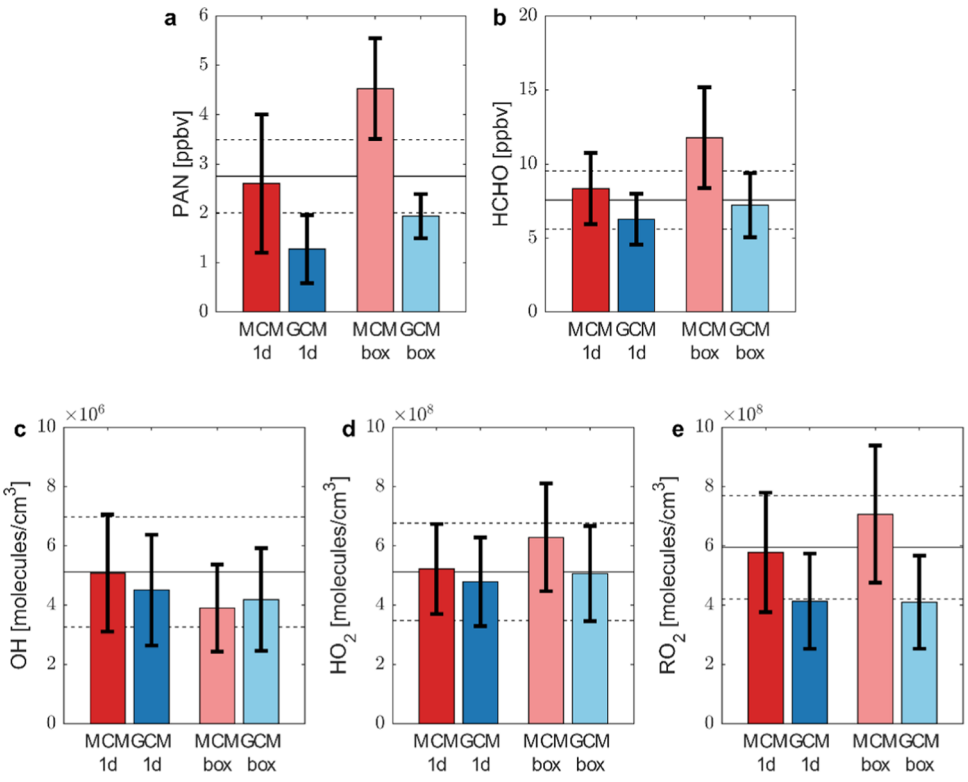

Figure 1. Observed and simulated daytime (8 am to 8 pm) average concentrations. (a) PAN, (b) HCHO, (c) OH, (d) HO_2, and (e) RO_2. The solid and dashed black horizontal lines show the observed mean and standard deviation, respectively. The color bars show the corresponding simulated averages of the surface layer in 1-D MCM and 1-D GCM and the averages of box MCM and box GCM models, respectively, with their standard deviations shown in vertical black lines.

The spin-up effect on the model evaluation is relatively small because the initial condition at the end of the spin-up only affects the simulations of species not measured in the first few days. The species of interest have short lifetimes and are affected negligibly.

We compare the simulations of HCHO, PAN, and free radicals in the four models in light of the observations (Section 3.1) and examine the amplification effects by OVOC photolysis on the production of OH, HO_2, RO_2, and ozone (Section 3.2). In Section 3.3, we investigate the sensitivity of radical cycling to the uptake coefficient of HO_2. We discuss the implications of the modeling analysis in Section 4.

3. RESULTS

3.1. Formaldehyde (HCHO), Peroxyacetyl Nitrate (PAN), and Free Radicals. Wangdu is a rural site (Figure S1), 170, 180, and 90 km from Beijing, Tianjin, and Shijiazhuang, respectively. However, the in situ observations during the CAREBEIJING-2014 campaign showed that the site was fairly polluted in summer.[32,34,48] We apply box and 1-D models to simulate short-lived daytime HCHO, PAN, and free-radical concentrations in light of the observations to understand the effects of boundary-layer mixing. We also use two chemical mechanisms. The Master Chemical Mechanism (MCM)[22−27] is much more detailed than the GEOS-Chem condensed mechanism (GCM).[38] However, the MCM is computationally too expensive to be regularly used in 3-D regional and global modeling of photochemistry. CARE-BEIJING-2014 observations of O_3, CO, CH_4, H_2O, NO, NO_2, HONO, VOCs, Cl_2, $ClNO_2$, temperature, pressure, and aerosol surface area are applied to constrain the model simulations.

To evaluate model-simulated photochemistry, short-lived chemical species are most useful, such as free radicals.[48] HCHO and PAN also have short lifetimes (0.5−2 h at noon) in summer near the surface due to photolysis and thermolysis, respectively, and their observations provide useful constraints on simulated photochemistry.[7] The daytime variations of short-lived species are strongly affected by solar radiation, which the model can reasonably capture. We compare the daytime (8 am to 8 pm) averages of box and 1-D model-simulated HCHO, PAN, OH, HO_2, and RO_2 concentrations with two chemical mechanisms (MCM and GCM) to the observations (Figure 1). The 1-D model simulation with the MCM shows the best agreement with the observations. The different characteristics between chemical mechanisms and between box and 1-D modeling are shown clearly in PAN simulations. The MCM models predict 2−3 times more PAN than GCM models. Vertical mixing in the 1-D model reduces PAN concentrations near the surface,[7] and therefore, simulated average PAN concentrations are 52−74% higher in the box than in 1-D models using the same chemical mechanism. Similar differences, but to a lesser extent, can be found for the simulations of HCHO, HO_2, and RO_2. In contrast, simulated daytime average OH concentrations are similar among box MCM and 1-D and box GCM models. The more detailed comparison (Figure S5) shows similar results. The vertical profile and the time series of the five species can be found in Figures S6 and S7. The previous study by Fuchs et al. shows that the observed level of OH reactivity can be explained by measured species.[48] Using their data, we find that the model-

https://doi.org/10.1021/acs.est.1c04489
Environ. Sci. Technol. 2021, 55, 13718−13727

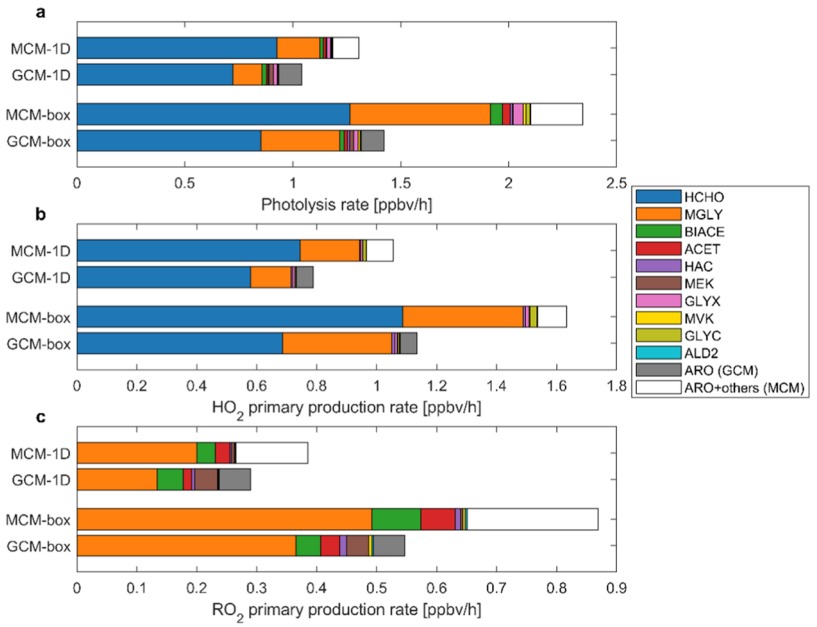

Figure 2. Daytime average results for the box models and the surface layer of the 1-D models. (a) OVOC photolysis rate, (b) HO_2 primary production rate from photolysis of OVOCs, and (c) RO_2 primary production rate from photolysis of OVOCs. The OVOC species simulated by both MCM and GCM mechanisms are formaldehyde (HCHO), methylglyoxal (MGLY), biacetyl (BIACE), acetone (ACET), hydroxy acetone (HAC), methyl ethyl ketone (MEK), glyoxal (GLYX), methyl vinyl ketone (MVK), glycolaldehyde (GLYC), and acetaldehyde (CH_3CHO). The contributions by the photolysis of aromatics (ARO) oxidation products can be tracked in the GCM but not in MCM. Therefore, the contributions by the photolysis of aromatics oxidation products and all of the OVOCs not explicitly simulated in the GCM are lumped as "ARO + others".

estimated daytime OH production, which is largely insensitive to the model setup, is comparable to the observation-derived OH loss (Figure S8).

Most of the differences among MCM and GCM modeling results discussed above are due to the higher production of OVOCs in the former. Photochemistry of OVOCs such as methylglyoxal significantly affects peroxy radical and PAN concentrations.[7,17] Fast-reactive VOC and OVOC concentrations decrease with altitude in the 1-D model since the emission sources are near the surface. Therefore, vertical mixing in daytime tends to decrease the concentrations of peroxy radical, PAN, and HCHO concentrations in 1-D than box model simulations.[7] In the surface layer of the 1-D MCM model, the vertical transport accounts for 41% of the total OVOC loss and the fractions can be as high as 53−82% for fast-reacting OVOCs (Table S4). The effects of OVOCs on OH concentrations are more complex. The enhancement of HO_2 tends to increase OH through the reaction of HO_2 and NO. On the other hand, the reaction of OH with OVOCs decreases OH, leading to a buffering effect on OH by the OVOC increase in the MCM than GCM. Due to this buffering effect, the daytime average OH concentrations of 1-D GCM and box GCM and MCM models are similar, lower than the 1-D MCM model.

The observed daytime average of PAN at 2.8 ppbv is lower than in polluted Beijing but much higher than background sites.[7,49−51] The 1-D MCM model simulates well the observed mean and standard deviation of the measurements. The 1-D GCM model underestimates the measured average by 54%, clearly having a low bias. The box GCM model results are higher than the 1-D GCM model but are still too low compared to the measurements. The box MCM model, on the other hand, overestimates the observed average by 65%. The much larger enhancements of PAN concentrations in the box than in 1-D model using the MCM than GCM reflect the much larger production and export of OVOCs from the surface layer to the boundary layer since the surface OVOC precursors in the models are the same, constrained by the available observations (Table S4). The model sensitivities to vertical mixing (1-D compared to box model) and chemical mechanism are much higher for PAN than for HCHO, reflecting, in part, the higher sensitivities of methylglyoxal than HCHO, which we will discuss further in Figure 2, and, in part, the vertical gradient of NO_x in the boundary layer.[7,42]

The observed daytime HCHO average at 7.6 ppbv, comparable to the summertime observation in Beijing,[52] is simulated well by the 1-D MCM model with a small high bias of 10%. The box MCM model overestimates the observations by 55%. As in the case of PAN, the effect of vertical mixing is larger in the MCM than that in the GCM. The GCM simulations are lower than the observations although the box GCM results are higher than the observations. Since OVOCs such as HCHO are among the major precursors to peroxy radicals,[6,53,54] the comparisons of model results with measured peroxy radical concentrations follow the pattern of HCHO but with smaller differences. The observed mean daytime concentrations of HO_2 and RO_2 are 5.1×10^8 and 5.9×10^8 molecules cm^{-3}, respectively. The simulated HO_2 concentrations by the four models are within the observed standard deviations of the observations. The MCM models simulate the observed RO_2 better than the 30% underestimates by the GCM 1-D and box models. The underestimation of RO_2 radicals is also found in a previous box model study using another simplified mechanism.[32] The observed daytime average OH concentration is 5.1×10^6 molecules cm^{-3}. The 1-D MCM-simulated OH is in agreement with the observations, while the simulations are lower by 12−24% in GCM and box MCM models. The model difference in OH is

https://doi.org/10.1021/acs.est.1c04489
Environ. Sci. Technol. 2021, 55, 13718−13727

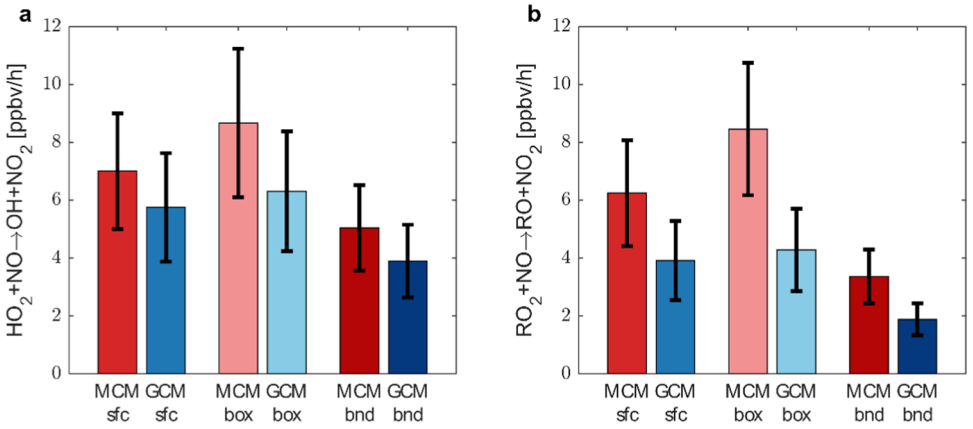

Figure 3. Simulated daytime average ozone production rates. (a) The ozone production from HO_2 oxidizing NO; (b) the ozone production from RO_2 oxidizing NO. The results are for the surface layer in the 1-D MCM, the surface layer in the 1-D GCM, box MCM, box GCM, the boundary-layer average in the 1-D MCM and the boundary-layer average in the 1-D GCM models, with the standard deviation shown in black lines. Since ozone is specified as observed, its losses through photolysis and dry deposition in the surface layer are the same in all models.

less than those of peroxy radicals due, in part, to the buffering effect of OVOCs and, in part, to the primary OH sources from the photolysis of HONO and the reaction of $O(^1D)$ and H_2O, which are the same in all model simulations.

3.2. Chemical Production of OVOCs and Their Contributions to the Production of Peroxy Radicals.

Figure S9 shows the radical budgets in the model simulations. Among the primary radical sources, peroxy radical production rates through photolysis of OVOCs differ the most in the model simulations. Photolysis of OVOCs accounts for one-third of the total primary radical production in the 1-D models and nearly half in the box models and in the boundary layer of the 1-D models (Figure S10). Furthermore, sensitivity simulations indicate that the photolytic production of HO_2 and RO_2 from OVOCs has a large impact on radical concentrations, ozone production rate, and the concentrations of PAN and HCHO (Figure S11). Figure 1 also shows that the MCM produces much higher OVOC and peroxy radical concentrations than the GCM. The latter is a condensed mechanism,[38] which tracks 25 OVOC species compared to ~900 OVOC species in the MCM. A direct consequence of higher OVOCs in the MCM than in GCM is the larger primary sources of radicals, which lead to higher peroxy radical concentrations and consequently higher production rates of ozone.[5−7]

Figure 2 shows the photolysis and primary HO_2 and RO_2 production rates by OVOC species in the four models. Compared to the GCM models, the MCM total photolysis rate is higher by 25% in the 1-D model and 65% in the box model. Among the simulated OVOC species in all simulations, the two species providing the largest primary sources of peroxy radicals are formaldehyde (HCHO) and methylglyoxal (MGLY), contributing >80% of the total OVOC photolysis in the four models. The 1-D MCM model produces 34% more HO_2 and 33% more RO_2 than the 1-D GCM model, and the box MCM model produces 44% more HO_2 and 59% more RO_2 than the box GCM model. HCHO and MGLY remain the largest two sources for HO_2 production, contributing >90% of the total HO_2 photolytic production in all four models. Since HCHO does not produce RO_2 in photolysis, MGLY becomes the largest source for RO_2 production, contributing 52% in the 1-D MCM model, 57% in the box MCM model, 46% in the 1-D GCM model, and 67% in the box GCM model. Ozonolysis is also a primary source of HO_2 and RO_2 radicals.[55] However, its contribution is relatively low in daytime compared to the photolysis of OVOCs (Figures S9 and S10). The total ozonolysis rate in the GCM is slower than that in MCM because the lumping of higher than C_3 alkenes with propene in the GCM is based on the reactivity of OH, not that of O_3.

The 1-D model results show differences between the MCM and GCM similar to box model results, but the calculated reaction rates in the surface layer are smaller, reflecting that vertical mixing decreases OVOC concentrations near the surface. The vertical mixing of OVOCs also implies that the higher OVOC production rates in the MCM than in GCM (Figures 1 and 2) affect the entire boundary layer. Quantitatively, the 1-D MCM model predicts faster OVOC photolysis and HO_2 and RO_2 production rates by 25, 34, and 33%, respectively, than the 1-D GCM model. The higher 1-D MCM HO_2 and RO_2 production rates are due primarily to methylglyoxal and the OVOC species not explicitly simulated in the GCM. The contribution by the latter is particularly large at 4% for HO_2 and 23% for RO_2. The contributions by biacetyl photolysis to the primary peroxy radical product are smaller in 1-D than box model simulations due to vertical mixing.

Chemical production of ozone is through the reactions of peroxy radicals with NO.[56] The higher primary productions of radicals (Figure 2) lead to significantly higher HO_2 and RO_2 concentrations in the MCM than in GCM (Figure 1), resulting in a higher production of ozone near the surface and in the boundary layer. As expected, the 1-D MCM model predicts a daytime average ozone production rate of 13.3 ppbv h^{-1} near the surface, 37% higher than the 9.7 ppbv h^{-1} in the 1-D GCM model (Figure 3). The reaction pathway through RO_2 contributes 6.3 ppbv h^{-1}, 60% higher in 1-D MCM than in the GCM model. It is larger than the MCM enhancement of 22% for the reaction pathway through HO_2. Box models predict higher ozone production rates but the relative differences between the MCM and GCM are similar to those of the 1-D models. The ratios of HO_2 to RO_2 pathways are 1:1 and 3:2 in MCM and GCM models, respectively. The corresponding ratios increase to 3:2 and 2:1 in the boundary layer. Both the relative and absolute contributions by the RO_2 pathway are larger in the MCM than in GCM models, reflecting the effect of significantly faster OVOC production in the MCM.

https://doi.org/10.1021/acs.est.1c04489
Environ. Sci. Technol. 2021, 55, 13718−13727

3.3. Sensitivity of Radical Cycling to the HO_2 Uptake Coefficient. The heterogeneous uptake of HO_2 on the aerosol surface is a sink of the active radicals and the dominant pathway for aerosols to affect ozone.[17] The uptake coefficient (γ) for HO_2 on the aerosol surface as high as 0.2 was used previously.[57] However, the Wangdu observation-derived uptake coefficient for HO_2 is 0.08.[58] We adopt this value in this study and include a high value of 0.2 in sensitivity tests. With a high aerosol surface area of ~1500 μm^2 cm^{-3} in Wangdu, the heterogeneous HO_2 uptake contributes an average daytime (8 am to 8 pm) radical loss of 1.1, 1.0, 1.6, and 1.1 ppbv h^{-1} in 1-D MCM, 1-D GCM, box MCM, and box GCM models, respectively (Figure S9). Although the uptake rate of HO_2 in the MCM models is faster than in the GCM models due to higher HO_2 concentrations, the sensitivity simulations on $\gamma(HO_2)$ indicate that the GCM model is more sensitive to the HO_2 aerosol uptake (Figure S12). With the $\gamma(HO_2)$ value changing from 0 to 0.2, the HO_2 concentrations are reduced by 23% in the GCM models, compared to 19% in MCM models. The OH concentration also shows a slightly higher sensitivity to $\gamma(HO_2)$ in the GCM models, with a reduction of 12%, compared to 10% in the MCM models. The RO_2 concentration is less sensitive to $\gamma(HO_2)$, with a reduction of 7−9 and 5−7% in the GCM and MCM models, respectively. PAN and HCHO concentrations are insensitive to $\gamma(HO_2)$. Since the ozone production rate is dependent on HO_2 and RO_2, the HO_2 uptake also affects the ozone production rate. In GCM models, changing the $\gamma(HO_2)$ value from 0 to 0.2 leads to a 14−15% decrease compared to 11−12% in MCM models, indicating that the condensed GCM tends to overestimate the effect of HO_2 aerosol uptake on O_3 concentrations due, in part, to slower radical cycling in the GCM than in MCM (Figure S9).

4. IMPLICATIONS

Although it is a rural site in China, the observations at the Wangdu site in the summer of 2014 show high pollutant concentrations and provide a comprehensive data set for evaluating the model representation of radical-driven photochemistry. We analyzed in detail the comparison of the MCM-to-GCM mechanism in this study. In the GCM, the rate constants are based on the measured kinetics data as much as possible as most of the other condensed mechanisms. A difficulty of condensed mechanism is that if the reaction rate constants and product yields for OVOC producing reactions are based on measured values in the same way as in the MCM, there will be VOC species and OVOC production pathways not represented in the condensed mechanism, which means that OVOC production will be underestimated. This problem can be solved by adjusting the rate constants and product yields to produce similar results as the MCM, in which case one must assume that the MCM mechanism is correct. The modeling analysis of observations of Wangdu indicates that the 1-D model results using the MCM are an improvement over the GCM. The potential biases in the other condensed chemical mechanisms therefore need to be further quantified. It is conceivable that some condensed chemical mechanisms may have lower biases for a given data set than found in this work. However, whether a condensed mechanism can match the performance of a detailed mechanism like MCM under varying ambient conditions in polluted urban and suburban regions requires new studies.

We find that the importance of the chemical production of OVOCs in photochemistry is manifested in several aspects. First, more OVOCs are produced near the surface due to fast-reacting VOCs such as isoprene, aromatics, alkenes, and high-molecular-weight alkanes. The lifetimes of OVOCs are hours comparable to vertical mixing of the boundary layer in daytime. Consequently, large amounts of OVOCs are exported from the surface layer to the rest of the boundary layer. The large production of OVOCs near the surface helps promote photochemistry in the whole boundary layer. Box models, which do not simulate the vertical mixing process, tend to overestimate OVOC concentrations and their effects on peroxy radicals, PAN, and ozone production near the surface by up to 76% compared to the observations and 1-D models.

Second, the condensed mechanisms are widely used in regional and global 3-D models because of their computational efficiency. Compared to the explicit MCM, which simulates over 900 OVOC species, the GCM resolves 25 OVOC species. Among the species simulated by both mechanisms in the 1-D models, the MCM predicts higher daytime HCHO (28%) and methylglyoxal (49%) than GCM near the surface, leading to 32 and 49% enhancements in HO_2 and RO_2 productions, respectively. The photolysis of OVOCs not explicitly simulated in the GCM accounts for 7% of the total primary radical source from OVOC photolysis, leading to moderate increases of HO_2 production by 4% near the surface and 8% in the boundary layer. The corresponding increases for RO_2 production are much higher at 23 and 38%, respectively. Third, the much higher OVOC production in the MCM leads to a lower sensitivity of simulated peroxy radical concentrations to the aerosol loss of HO_2.

Finally, condensed mechanisms have been widely used in air quality policy studies.[46,59,60] The higher OVOC production in the MCM than in GCM indicates that the primary radical sources in the 3-D air quality models are likely underestimated, leading to a lower sensitivity of simulated ozone production to NO_x emissions. Figure 4 illustrates the sensitivity of the average daytime ozone production rate to the changes in NO_x emissions. Similar results are found if the net ozone production

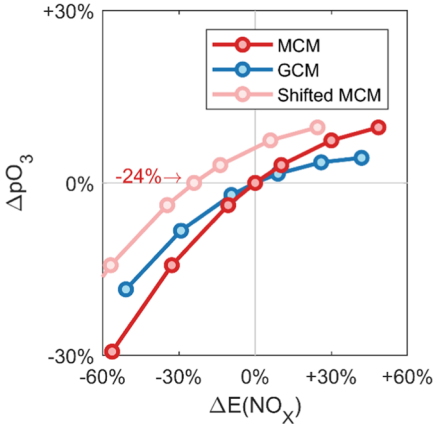

Figure 4. Sensitivities of the boundary-layer daytime mean ozone production rate to NO_x emission change. The dark red line shows the results for 1-D MCM models, and the blue line shows the results for 1-D GCM models. The emission rate is computed by the net NO_x chemical loss in the boundary layer. The light red line shows the MCM sensitivity data points with emission changes shifted 24% to the left. The shifted MCM sensitivity line is largely in parallel to the GCM result.

https://doi.org/10.1021/acs.est.1c04489
Environ. Sci. Technol. 2021, 55, 13718−13727

rate is used instead (Figure S13). The condensed GCM shows that the linear increase of ozone production due to increasing NO_x emission by a least-squares regression is 66% lower than the decrease of ozone production due to decreasing NO_x emission (Text S1). This asymmetry of ozone production sensitivity to NO_x emission change reflects a transition from NO_x-limited to VOC-limited chemical regime in ozone production.[17,56,61] In comparison, the ozone production sensitivity to NO_x emission in the MCM is higher and the asymmetry is reduced; the linear increase of ozone production due to increasing NO_x emission by least-squares regression is 57% lower than the decrease of ozone production due to decreasing NO_x emission. The difference is equivalent to shifting NO_x emissions by 24% higher in the MCM to match the ozone production sensitivity to NO_x in the GCM at the origin (Text S2). Therefore, the MCM model simulated ozone production regime is tilted more toward NO_x-limited than the GCM model. It implies that the 3-D air quality modeling may have a bias of underestimating the efficacy of NO_x emission reduction on controlling ozone in polluted urban and suburban regions of China. Further quantification of this bias for a specific region requires more measurements of OVOCs, particularly formaldehyde, methylglyoxal, and peroxy radicals (particularly RO_2) in addition to air quality monitoring data of ozone, CO, NO_x, and VOCs.

■ ASSOCIATED CONTENT

Supporting Information

The Supporting Information is available free of charge at https://pubs.acs.org/doi/10.1021/acs.est.1c04489.

Lumping process of the VOCs (Text S1); least-squares regression (Text S2); equivalent NO_x emission shift (Text S3); observation methods, time resolution, and 1-σ uncertainties for trace gases (Table S1); measured VOCs and the corresponding species name in MCM and GCM (Table S2); top height of the layers in 1-D models (Table S3); chemical and vertical transport losses of OVOCs in the 1-D MCM model (Table S4); polynomial fitting results (Table S5); location of Wangdu (Figure S1); model domain of WRF and REAM (Figure S2); boundary-layer height time series (Figure S3); comparison of the vertical diffusion coefficient (Figure S4); comparison of the simulated and observed radicals and OVOCs (Figure S5); comparison of the vertical profiles of PAN, HCHO, OH, HO_2, and RO_2 (Figure S6); comparison of PAN, HCHO, OH, HO_2, and RO_2 time series (Figure S7); comparison of the observed and simulated OH loss rates (Figure S8); simulated daytime radical budget (Figure S9); simulated ROx daytime source budget (Figure S10); sensitivity simulation on the effect from OVOC photolysis (Figure S11); sensitivity simulation on the effect from HO_2 uptake coefficient (Figure S12); and net ozone production sensitivity to NO_x emission (Figure S13) (PDF)

■ AUTHOR INFORMATION

Corresponding Author

Yuhang Wang − *School of Earth and Atmospheric Sciences, Georgia Institute of Technology, Atlanta, Georgia 30332, United States;* orcid.org/0000-0002-7290-2551; Email: yuhang.wang@eas.gatech.edu

Authors

Hang Qu − *School of Earth and Atmospheric Sciences, Georgia Institute of Technology, Atlanta, Georgia 30332, United States;* orcid.org/0000-0002-2924-2826

Ruixiong Zhang − *School of Earth and Atmospheric Sciences, Georgia Institute of Technology, Atlanta, Georgia 30332, United States*

Xiaoxi Liu − *School of Earth and Atmospheric Sciences, Georgia Institute of Technology, Atlanta, Georgia 30332, United States*

Lewis Gregory Huey − *School of Earth and Atmospheric Sciences, Georgia Institute of Technology, Atlanta, Georgia 30332, United States;* orcid.org/0000-0002-0518-7690

Steven Sjostedt − *School of Earth and Atmospheric Sciences, Georgia Institute of Technology, Atlanta, Georgia 30332, United States; Cooperative Institute for Research in Environmental Sciences, University of Colorado, Boulder, Boulder, Colorado 80309, United States; Earth System Research Laboratory, National Oceanic and Atmospheric Administration, Boulder, Colorado 80305, United States*

Limin Zeng − *State Key Joint Laboratory of Environmental Simulation and Pollution Control, College of Environmental Sciences and Engineering, Peking University, Beijing 100871, China*

Keding Lu − *State Key Joint Laboratory of Environmental Simulation and Pollution Control, College of Environmental Sciences and Engineering, Peking University, Beijing 100871, China;* orcid.org/0000-0001-9425-9520

Yusheng Wu − *State Key Joint Laboratory of Environmental Simulation and Pollution Control, College of Environmental Sciences and Engineering, Peking University, Beijing 100871, China*

Min Shao − *State Key Joint Laboratory of Environmental Simulation and Pollution Control, College of Environmental Sciences and Engineering, Peking University, Beijing 100871, China; Institute for Environmental and Climate Research, Jinan University, Guangzhou 511443, China*

Min Hu − *State Key Joint Laboratory of Environmental Simulation and Pollution Control, College of Environmental Sciences and Engineering, Peking University, Beijing 100871, China;* orcid.org/0000-0003-4816-9123

Zhaofeng Tan − *State Key Joint Laboratory of Environmental Simulation and Pollution Control, College of Environmental Sciences and Engineering, Peking University, Beijing 100871, China; Institute of Energy and Climate Research, IEK-8: Troposphere, Forschungszentrum Jülich GmbH, Jülich 52425, Germany;* orcid.org/0000-0002-3808-1964

Hendrik Fuchs − *Institute of Energy and Climate Research, IEK-8: Troposphere, Forschungszentrum Jülich GmbH, Jülich 52425, Germany;* orcid.org/0000-0003-1263-0061

Sebastian Broch − *Institute of Energy and Climate Research, IEK-8: Troposphere, Forschungszentrum Jülich GmbH, Jülich 52425, Germany*

Andreas Wahner − *Institute of Energy and Climate Research, IEK-8: Troposphere, Forschungszentrum Jülich GmbH, Jülich 52425, Germany*

Tong Zhu − *State Key Joint Laboratory of Environmental Simulation and Pollution Control, College of Environmental Sciences and Engineering, Peking University, Beijing 100871, China;* orcid.org/0000-0002-2752-7924

Yuanhang Zhang − *State Key Joint Laboratory of Environmental Simulation and Pollution Control, College of*

Environmental Sciences and Engineering, Peking University, Beijing 100871, China

Complete contact information is available at: https://pubs.acs.org/10.1021/acs.est.1c04489

Author Contributions

H.Q. and Y.W. designed the study. H.Q. performed the analysis and calculation. R.Z. conducted the WRF simulation. X.L., L.G.H., and S.S. measured halogen species and PAN. L.Z., K.L., Y.W., M.S., and M.H. measured the concentrations of other trace gases, VOCs, and aerosols. H.F., S.B., and A.W. measured the concentrations of hydroxyl and peroxy radicals. Y.Z. and T.Z. supervised the field campaign. H.Q. and Y.W. wrote and all coauthors reviewed the paper.

Notes

The authors declare no competing financial interest.

■ ACKNOWLEDGMENTS

This work was supported by the National Science Foundation Atmospheric Chemistry Program (grant 1743401). The authors thank the science teams of the Wangdu 2014 campaign. The Wangdu 2014 campaign was funded by the National Natural Science Foundation of China (major programs 21190052, 41421064, and 21522701), the Strategic Priority Research Program of the Chinese Academy of Sciences (grant XDB05010500), the Collaborative Innovation Center for Regional Environmental Quality, and the EU-project AMIS (Fate and Impact of Atmospheric Pollutants, PIRSES-GA-2011-295132). The authors thank Dr. Andreas Hofzumahaus and Dr. Birger Bohn for the comments on the manuscript and the measurement of the photolysis frequencies.

■ REFERENCES

(1) Shim, C.; Wang, Y.; Singh, H. B.; Blake, D. R.; Guenther, A. B. Source characteristics of oxygenated volatile organic compounds and hydrogen cyanide. *J. Geophys. Res.* **2007**, *112*, No. D10305.

(2) Yang, M.; Beale, R.; Liss, P.; Johnson, M.; Blomquist, B.; Nightingale, P. Air-sea fluxes of oxygenated volatile organic compounds across the Atlantic Ocean. *Atmos. Chem. Phys.* **2014**, *14*, 7499−7517.

(3) Mellouki, A.; Wallington, T. J.; Chen, J. Atmospheric chemistry of oxygenated volatile organic compounds: impacts on air quality and climate. *Chem. Rev.* **2015**, *115*, 3984−4014.

(4) Schlundt, C.; Tegtmeier, S.; Lennartz, S. T.; Bracher, A.; Cheah, W.; Kruger, K.; Quack, B.; Marandino, C. A. Oxygenated volatile organic carbon in the western Pacific convective center: ocean cycling, air-sea gas exchange and atmospheric transport. *Atmos. Chem. Phys.* **2017**, *17*, 10837−10854.

(5) Singh, H. B.; Kanakidou, M.; Crutzen, J. P.; Jacob, D. J. High concentrations and photochemical fate of oxygenated hydrocarbons in the global troposphere. *Nature* **1995**, *378*, 50−54.

(6) Liu, Z.; Wang, Y.; Gu, D.; Zhao, C.; Huey, L. G.; Stickel, R.; Liao, J.; Shao, M.; Zhu, T.; Zeng, L.; Amoroso, A.; Costabile, F.; Chang, C. C.; Liu, S. C. Summertime photochemistry during CAREBeijing-2007: RO_X budgets and O_3 formation. *Atmos. Chem. Phys.* **2012**, *12*, 7737−7752.

(7) Liu, Z.; Wang, Y.; Gu, D.; Zhao, C.; Huey, L. G.; Stickel, R.; Liao, J.; Shao, M.; Zhu, T.; Zeng, L.; Liu, S. C.; Chang, C. C.; Amoroso, A.; Costabile, F. Evidence of reactive aromatics as a major source of peroxyacetyl nitrate over China. *Environ. Sci. Technol.* **2010**, *44*, 7017−7022.

(8) Brunekreef, B.; Holgate, S. T. Air pollution and health. *Lancet* **2002**, *360*, 1233−1242.

(9) Reich, P. B.; Amundson, R. G. Ambient levels of ozone reduce net photosynthesis in tree and crop species. *Science* **1985**, *230*, 566−570.

(10) Fischer, E. V.; Jacob, D. J.; Yantosca, R. M.; Sulprizio, M. P.; Millet, D. B.; Mao, J.; Paulot, F.; Singh, H. B.; Roiger, A.; Ries, L.; Talbot, R. W.; Dzepina, K.; Deolal, S. P. Atmospheric peroxyacetyl nitrate (PAN): a global budget and source attribution. *Atmos. Chem. Phys.* **2014**, *14*, 2679−2698.

(11) Singh, H. B.; Hanst, P. L. Peroxyacetyl nitrate (PAN) in the unpolluted atmosphere: an important reservoir for nitrogen oxides. *Geophys. Res. Lett.* **1981**, *8*, 941−944.

(12) Kokkola, H.; Yli-Pirila, P.; Vesterinen, M.; Korhonen, H.; Keskinen, H.; Romakkaniemi, S.; Hao, L.; Kortelainen, A.; Joutsensaari, J.; Worsnop, D. R.; Virtanen, A.; Lehtinen, K. E. J. The role of low volatile organics on secondary organic aerosol formation. *Atmos. Chem. Phys.* **2014**, *14*, 1689−1700.

(13) Hazra, M. K.; Francisco, J. S.; Sinha, A. Hydrolysis of glyoxal in water-restricted environments: formation of organic aerosol precursors through formic acid catalysis. *J. Phys. Chem. A* **2014**, *118*, 4095−4105.

(14) Li, J.; Mao, J.; Min, K. E.; Washenfelder, R. A.; Brown, S. S.; Kaiser, J.; Keutsch, F. N.; Volkamer, R.; Wolfe, G. M.; Hanisco, T. F.; Pollack, I. B.; Ryerson, T. B.; Graus, M.; Gilman, J. B.; Lerner, B. M.; Warneke, C.; de Gouw, J. A.; Middlebrook, A. M.; Liao, J.; Welti, A.; Henderson, B. H.; McNeill, V. F.; Hall, S. R.; Ullmann, K.; Donner, L. J.; Paulot, F.; Horowitz, L. W. Observational constraints on glyoxal production from isoprene oxidation and its contribution to organic aerosol over the Southeast United States. *J. Geophys. Res.: Atmos.* **2016**, *121*, 9849−9861.

(15) Read, K. A.; Carpenter, L. J.; Arnold, S. R.; Beale, R.; Nightingale, P. D.; Hopkins, J. R.; Lewis, A. C.; Lee, J. D.; Mendes, L.; Pickering, S. J. Multiannual observations of acetone, methanol, and acetaldehyde in remote tropical Atlantic air: implications for atmospheric OVOC budgets and oxidative capacity. *Environ. Sci. Technol.* **2012**, *46*, 11028−11039.

(16) Jaeglé, L.; Shah, V.; Thornton, J. A.; Lopez-Hilfiker, F. D.; Lee, B. H.; McDuffie, E. E.; Fibiger, D.; Brown, S. S.; Veres, P.; Sparks, T. L.; Ebben, C. J.; Wooldridge, P. J.; Kenagy, H. S.; Cohen, R. C.; Weinheimer, A. J.; Campos, T. L.; Montzka, D. D.; Digangi, J. P.; Wolfe, G. M.; Hanisco, T.; Schroder, J. C.; Campuzano-Jost, P.; Day, D. A.; Jimenez, J. L.; Sullivan, A. P.; Guo, H.; Weber, R. J. Nitrogen Oxides Emissions, Chemistry, Deposition, and Export Over the Northeast United States During the WINTER Aircraft Campaign. *J. Geophys. Res.: Atmos.* **2018**, *123*, 12368−12393.

(17) Liu, Z.; Wang, Y.; Vrekoussis, M.; Richter, A.; Wittrock, F.; Burrows, J. P.; Shao, M.; Chang, C. C.; Liu, S. C.; Wang, H.; Chen, C. Exploring the missing source of glyoxal (CHOCHO) over China. *Geophys. Res. Lett.* **2012**, *39*, No. L10812.

(18) Karl, T.; Striednig, M.; Graus, M.; Hammerle, A.; Wohlfahrt, G. Urban flux measurements reveal a large pool of oxygenated volatile organic compound emissions. *Proc. Natl. Acad. Sci. U.S.A.* **2018**, *115*, 1186−1191.

(19) Harkey, M.; Holloway, T.; Kim, E. J.; Baker, K. R.; Henderson, B. Satellite Formaldehyde to Support Model Evaluation. *J. Geophys. Res.: Atmos.* **2020**, *126*, No. e2020JD032881.

(20) Miller, C. C.; Jacob, D. J.; Marais, E. A.; Yu, K.; Travis, K. R.; Kim, P. S.; Fisher, J. A.; Zhu, L.; Wolfe, G. M.; Hanisco, T. F.; Keutsch, F. N.; Kaiser, J.; Min, K. E.; Brown, S. S.; Washenfelder, R. A.; Abad, G. G.; Chance, K. Glyoxal yield from isoprene oxidation and relation to formaldehyde: chemical mechanism, constraints from SENEX aircraft observations, and interpretation of OMI satellite data. *Atmos. Chem. Phys.* **2017**, *17*, 8725−8738.

(21) Li, J.; Zhang, M.; Tang, G.; Wu, F.; Alvarado, L. M. A.; Vrekoussis, M.; Richter, A.; Burrows, J. P. Investigating missing sources of glyoxal over China using a regional air quality model (RAMS-CMAQ). *J. Environ. Sci.* **2018**, *71*, 108−118.

(22) Jenkin, M. E.; Saunders, S. M.; Pilling, M. J. The tropospheric degradation of volatile organic compounds: a protocol for mechanism development. *Atmos. Environ.* **1997**, *31*, 81−104.

(23) Saunders, S. M.; Jenkin, M. E.; Derwent, R. G.; Pilling, M. J. Protocol for the development of the Master Chemical Mechanism, MCM v3 (Part A): tropospheric degradation of non-aromatic volatile organic compounds. *Atmos. Chem. Phys.* **2003**, *3*, 161−180.
(24) Jenkin, M. E.; Saunders, S. M.; Wagner, V.; Pilling, M. J. Protocol for the development of the Master Chemical Mechanism, MCM v3 (Part B): tropospheric degradation of aromatic volatile organic compounds. *Atmos. Chem. Phys.* **2003**, *3*, 181−193.
(25) Bloss, C.; Wagner, V.; Jenkin, M. E.; Volkamer, R.; Bloss, W. J.; Lee, J. D.; Heard, D. E.; Wirtz, K.; Martin-Reviejo, M.; Rea, G.; Wenger, J. C.; Pilling, M. J. Development of a detailed chemical mechanism (MCMv3.1) for the atmospheric oxidation of aromatic hydrocarbons. *Atmos. Chem. Phys.* **2005**, *5*, 641−664.
(26) Jenkin, M. E.; Wyche, K. P.; Evans, C. J.; Carr, T.; Monks, P. S.; Alfarra, M. R.; Barkey, M. H.; McFiggans, G. B.; Young, J. C.; Rickard, A. R. Development and chamber evaluation of the MCM v3.2 degradation scheme for β-caryophyllene. *Atmos. Chem. Phys.* **2012**, *12*, 5275−5308.
(27) Jenkin, M. E.; Young, J. C.; Rickard, A. R. The MCM v3.3.1 degradation scheme for isoprene. *Atmos. Chem. Phys.* **2015**, *15*, 11433−11459.
(28) Zhang, Y.; Wang, Y.; Chen, G.; Smeltzer, C.; Crawford, J.; Olson, J.; Szykman, J.; Weinheimer, A. J.; Knapp, D. J.; Montzka, D. D.; Wisthaler, A.; Mikoviny, T.; Fried, A.; Diskin, G. Large vertical gradient of reactive nitrogen oxides in the boundary layer: Modeling analysis of DISCOVER-AQ 2011 observations. *J. Geophys. Res.: Atmos.* **2016**, *121*, 1922−1934.
(29) Liu, Y.; Lu, K.; Dong, H.; Li, X.; Cheng, P.; Zou, Q.; Wu, Y.; Liu, X.; Zhang, Y. In situ monitoring of atmospheric nitrous acid based on multi-pumping flow system and liquid waveguide capillary cell. *J. Environ. Sci.* **2016**, *43*, 273−284.
(30) Wang, M.; Zeng, L.; Lu, S.; Shao, M.; Liu, X.; Yu, X.; Chen, W.; Yuan, B.; Zhang, Q.; Hu, M.; Zhang, Z. Development and validation of a cryogen-free automatic gas chromatograph system (GC-MS/FID) for online measurements of volatile organic compounds. *Anal. Methods* **2014**, *6*, 9424−9434.
(31) Liu, X.; Qu, H.; Huey, L. G.; Wang, Y.; Sjostedt, S.; Zeng, L.; Lu, K.; Wu, Y.; Hu, M.; Shao, M.; Zhu, T.; Zhang, Y. High levels of daytime molecular chlorine and nitryl chloride at a rural site on the North China Plain. *Environ. Sci. Technol.* **2017**, *51*, 9588−9595.
(32) Tan, Z.; Fuchs, H.; Lu, K.; Hofzumahaus, A.; Bohn, B.; Broch, S.; Dong, H.; Gomm, S.; Haseler, R.; He, L.; Holland, F.; Li, X.; Liu, Y.; Lu, S.; Rohrer, F.; Shao, M.; Wang, B.; Wang, M.; Wu, Y.; Zeng, L.; Zhang, Y.; Wahner, A.; Zhang, Y. Radical chemistry at a rural site (Wangdu) in the North China Plain: observation and model calculations of OH, HO_2 and RO_2 radicals. *Atmos. Chem. Phys.* **2017**, *17*, 663−690.
(33) Bohn, B.; Corlett, G. K.; Gillmann, M.; Sanghavi, S.; Stange, G.; Tensing, E.; Vrekoussis, M.; Bloss, W. J.; Clapp, L. J.; Kortner, M.; Dorn1, H. P.; Monks, P. S.; Platt, U.; Plass-Dulmer, C.; Mihalopoulos, N.; Heard, D. E.; Clemitshaw, K. C.; Meixner, F. X.; Prevot, A. S. H.; Schmitt, R. Photolysis frequency measurement techniques: results of a comparison within the ACCENT project. *Atmos. Chem. Phys.* **2008**, *8*, 5373−5391.
(34) Wang, Y.; Chen, Z.; Wu, Q.; Liang, H.; Huang, L.; Li, H.; Lu, K.; Wu, Y.; Dong, H.; Zeng, L.; Zhang, Y. Observation of atmospheric peroxides during Wangdu campaign 2014 at a rural site in the North China Plain. *Atmos. Chem. Phys.* **2016**, *16*, 10985−11000.
(35) Shareef, M. M.; Husain, T.; Alharbi, B. Studying the Effect of Different Gas-Phase Chemical Kinetic Mechanisms on the Formation of Oxidants, Nitrogen Compounds and Ozone in Arid Regions. *J. Environ. Prot.* **2019**, *10*, 1006−1031.
(36) Safronov, A. N.; Shtabkin, Y. A.; Berezina, E. V.; Skorokhod, A. I.; Rakitin, V. S.; Beliov, I. B.; Elansky, N. F. Isoprene, Methyl Vinyl Ketone and Methhacrolein from TROICA-12 Measurements and WRF-CHEM and GEOS-CHEM Simulations in the Far East Region. *Atmosphere* **2019**, *10*, No. 152.
(37) Yu, S.; Mathur, R.; Sarwar, G.; Kang, D.; Tong, D.; Pouliot, G.; Pleim, J. Eta-CMAQ air quality forecasts for O_3 and related species using three different photochemical mechanisms (CB4, CB05, SAPRC-99): comparisons with measurements during the 2004 ICARTT study. *Atmos. Chem. Phys.* **2010**, *10*, 3001−3025.
(38) Bey, I.; Jacob, D. J.; Yantosca, R. M.; Logan, J. A.; Field, B. D.; Fiore, A. M.; Li, Q.; Liu, H. Y.; Mickley, L. J.; Schultz, M. G. Global modeling of tropospheric chemistry with assimilated meteorology: Model description and evaluation. *J. Geophys. Res.* **2001**, *106*, 23073−23095.
(39) Wild, O.; Zhu, X.; Prather, M. J. Fast-J: Accurate simulation of in- and below-cloud photolysis in tropospheric chemical models. *J. Atmos. Chem.* **2000**, *37*, 245−282.
(40) Jacobson, M. Z.; Turco, R. P. SMVGEAR: A sparse-matrix, vectorized gear code for atmospheric models. *Atmos. Environ.* **1994**, *28*, 273−284.
(41) Saha, S.; Moorthi, S.; Wu, X.; Wang, J.; Nadiga, S.; Tripp, P.; Behringer, D.; Hou, Y. T.; Chuang, H. Y.; Iredell, M.; Ek, M.; Meng, J.; Yang, R.; Mendez, M. P.; van den Dool, H.; Zhang, Q.; Wang, W.; Chen, M.; Becker, E. The NCEP Climate Forecast System Version 2. *J. Clim.* **2014**, *27*, 2185−2208.
(42) Zhang, Y.; Wang, Y.; Chen, G.; Smeltzer, C.; Crawford, J.; Olson, J.; Szykman, J.; Weinheimer, A. J.; Knapp, D. J.; Montzka, D. D.; Wisthaler, A.; Mikoviny, T.; Fried, A.; Diskin, G. Large vertical Gradient of Reactive Nitrogen Oxides in the Boundary Layer: Modeling Analysis of DISCOVER-AQ 2011 Observations. *J. Geophys. Res.: Atmos.* **2016**, *121*, 1922−1934.
(43) Zhang, Q.; Streets, D.; Carmichael, G.; He, K.; Huo, H.; Kannari, A.; Klimont, Z.; Park, I. S.; Reddy, S.; Fu, J.; Chen, D.; Duan, L.; Lei, Y.; Wang, L.; Yao, Z. Asian emissions in 2006 for the NASA INTEX-B mission. *Atmos. Chem. Phys.* **2009**, *9*, 5131−5153.
(44) Guenther, A. B.; Jiang, X.; Heald, C. L.; Sakulyanontvittaya, T.; Duhl, T.; Emmons, L. K.; Wang, X. The Model of Emissions of Gases and Aerosols from Nature version 2.1 (MEGAN2.1): an extended and updated framework for modeling biogenic emissions. *Geosci. Model Dev.* **2012**, *5*, 1471−1552.
(45) Zhang, R.; Wang, Y.; Smeltzer, C.; Qu, H.; Koshak, W.; Boersma, K. F. Comparing OMI-based and EPA AQS in situ NO2 trends: Towards understanding surface NOx emission changes. *Atmos. Meas. Tech.* **2018**, *11*, 3955−3967.
(46) Zhang, R.; Wang, Y.; He, Q.; Chen, L.; Zhang, Y.; Qu, H.; Smeltzer, C.; Li, J.; Alvarado, L. M. A.; Vrekoussis, M.; Richter, A.; Wittrock, F.; Burrows, J. P. Enhanced trans-Himalaya Pollution transport to the Tibetan Plateau by cut-off low systems. *Atmos. Chem. Phys.* **2017**, *17*, 3083−3095.
(47) Gu, D.; Wang, Y.; Smeltzer, C.; Boersma, K. F. Anthropogenic emissions of NOx over China: Reconciling the difference of inverse modeling results using GOME-2 and OMI measurements. *J. Geophys. Res.: Atmos.* **2014**, *119*, 7732−7740.
(48) Fuchs, H.; Tan, Z.; Lu, K.; Bohn, B.; Broch, S.; Brown, S. S.; Dong, H.; Gomm, S.; Haseler, R.; He, L.; Hofzumahaus, A.; Holland, F.; Li, X.; Liu, Y.; Lu, S.; Min, K. E.; Rohrer, F.; Shao, M.; Wang, B.; Wang, M.; Wu, Y.; Zeng, L.; Zhang, Y.; Wahner, A.; Zhang, Y. OH reactivity at a rural site (Wangdu) in the North China Plain: contributions from OH reactants and experimental OH budget. *Atmos. Chem. Phys.* **2017**, *17*, 645−661.
(49) Phillips, G. J.; Pouvesle, N.; Thieser, J.; Schuster, G.; Axinte, R.; Fischer, H.; Williams, J.; Lelieveld, J.; Crowley, J. N. Peroxyacetyl nitrate (PAN) and peroxyacetic acid (PAA) measurements by iodide chemical ionisation mass spectrometry: first analysis of results in the boreal forest and implications for the measurement of PAN fluxes. *Atmos. Chem. Phys.* **2013**, *13*, 1129−1139.
(50) Lee, G.; Choi, H. S.; Lee, T.; Choi, J.; Park, J. S.; Ahn, J. Y. Variations of regional background peroxyacetyl nitrate in marine boundary layer over Baengyeong Island, South Korea. *Atmos. Environ.* **2012**, *61*, 533−541.
(51) Zhang, G.; Mu, Y.; Zhou, L.; Zhang, C.; Zhang, Y.; Liu, J.; Fang, S.; Yao, B. Summertime distributions of peroxyacetyl nitrate (PAN) and peroxypropionyl nitrate (PPN) in Beijing: Understanding the sources and major sink of PAN. *Atmos. Environ.* **2015**, *103*, 289−296.

https://doi.org/10.1021/acs.est.1c04489
Environ. Sci. Technol. 2021, 55, 13718−13727

(52) Qian, X.; Shen, H.; Chen, Z. Characterizing summer and winter carbonyl compounds in Beijing atmosphere. *Atmos. Environ.* **2019**, *214*, No. 116845.
(53) Xue, L.; Gu, R.; Wang, T.; Wang, X.; Saunders, S.; Blake, D.; Louie, P. K. K.; Luk, C. W. Y.; Simpson, I.; Xu, Z.; Wang, Z.; Gao, Y.; Lee, S.; Mellouki, A.; Wang, W. Oxidative capacity and radical chemistry in the polluted atmosphere of Hong Kong and Pearl River Delta region: analysis of a severe photochemical smog episode. *Atmos. Chem. Phys.* **2016**, *16*, 9891−9903.
(54) Griffith, S. M.; Hansen, R. F.; Dusanter, S.; Michoud, V.; Gilman, J. B.; Kuster, W. C.; Veres, P. R.; Graus, M.; de Gouw, J. A.; Roberts, J.; Young, C.; Washenfelder, R.; Brown, S. S.; Thalman, R.; Waxman, E.; Volkamer, R.; Tsai, C.; Stutz, J.; Flynn, J. H.; Grossberg, N.; Lefer, B.; Alvarez, S. L.; Rappenglueck, B.; Mielke, L. H.; Osthoff, H. D.; Stevens, P. S. Measurements of hydroxyl and hydroperoxyl radicals during CalNex-LA: Model comparisons and radical budgets. *J. Geophys. Res.: Atmos.* **2016**, *121*, 4211−4232.
(55) Johnson, D.; Marston, G. The gas-phase ozonolysis of unsaturated volatile organic compounds in the troposphere. *Chem. Soc. Rev.* **2008**, *37*, 699−716.
(56) Kleinman, L. I.; Daum, P. H.; Imre, D.; Lee, Y. N.; Nunnermacker, L. J.; Springston, S. R.; Weinstein-Lloyd, J.; Rudolph, J. Ozone production rate and hydrocarbon reactivity in 5 urban areas: A cause of high ozone concentration in Houston. *Geophys. Res. Lett.* **2002**, *29*, 105-1−105-4.
(57) Li, K.; Jacob, D. J.; Liao, H.; Shen, L.; Zhang, Q.; Bates, K. H. Anthropogenic drivers of 2013-2017 trends in summer surface ozone in China. *Proc. Natl. Acad. Sci. U.S.A.* **2019**, *116*, 422−427.
(58) Tan, Z.; Hofzumahaus, A.; Lu, K.; Brown, S. S.; Holland, F.; Huey, L. G.; Kiendler-Scharr, A.; Li, X.; Liu, X.; Ma, N.; Min, K. E.; Rohrer, F.; Shao, M.; Wahner, A.; Wang, Y.; Wiedensohler, A.; Wu, Y.; Wu, Z.; Zeng, L.; Zhang, Y.; Fuchs, H. No evidence for a significant impact of heterogeneous chemistry on radical concentrations in the North China Plain in summer 2014. *Environ. Sci. Technol.* **2020**, *54*, 5973−5979.
(59) Lee, Y. N.; Zhou, X.; Hallock, K. Atmospheric carbonyl compounds at a rural southeastern United States site. *J. Geophys. Res.* **1995**, *100*, 25933−25944.
(60) Yang, Q.; Wang, Y.; Zhao, C.; Liu, Z.; Gustafson, W. I., Jr.; Shao, M. NOx emission reduction and its effects on ozone during the 2008 Olympic Games. *Environ. Sci. Technol.* **2011**, *45*, 6404−6410.
(61) Li, J.; Wang, Y.; Qu, H. Dependence of summertime surface ozone on NO_X and VOC emissions over the United States: Peak time and value. *Geophys. Res. Lett.* **2019**, *46*, 3540−3550.

https://doi.org/10.1021/acs.est.1c04489
Environ. Sci. Technol. 2021, 55, 13718−13727